

# Quantum Spin Models from Flux Tubes in Correlated Topological Insulators

F. F. Assaad, M. Bercx, and M. Hohenadler

*Institut für Theoretische Physik und Astrophysik, Universität Würzburg, Am Hubland, 97074 Würzburg, Germany*

(Dated: May 28, 2022)

We demonstrate that spin fluxon states generated by  $\pi$  fluxes can be used in quantum Monte Carlo simulations to identify a correlated  $Z_2$  topological insulator. In the presence of repulsive electronic interactions, the spin fluxons form localized, low-energy spin-1/2 degrees of freedom with a distinct Curie law in the magnetic susceptibility. Electronic correlations generate a bosonic mode of magnetic excitons with tunable energy that act as exchange particles and mediate a dynamical spin-spin interaction of adjustable range and strength. In combination with the freedom to create almost arbitrary spin lattices, correlated topological insulators with  $\pi$  fluxes represent a novel kind of quantum simulator useful for numerical simulations and experiments.

PACS numbers: 03.65.Vf, 71.27.+a, 75.10.Jm, 03.67.Ac, 73.43.-f

Topological band insulators (TBIs) represent a novel state of matter characterized by a special band structure resulting, e.g., from strong spin-orbit (SO) interaction [1, 2]. Two-dimensional TBIs, or *quantum spin Hall (QSH) insulators*, have deep connections with the quantum Hall effect, including the coexistence of a bulk band gap and metallic edges, absence of symmetry breaking, and a mathematical classification [3]. The QSH insulator preserves time reversal symmetry (TRS)—providing protection against interactions and disorder [4–6]—and has been realized in HgTe quantum wells [7, 8].

TBIs with strong electronic correlations are in the focus of current research. Intriguing concepts include electron fractionalization [9, 11–13], spin liquids [13–15], and topological Mott insulators [16, 17]. A central problem is the question of how to identify a TBI directly from bulk properties. Experimentally, this issue emerges in the absence of sharp edges in proposed cold atom realizations [18, 19]. The original  $Z_2$  classification is only valid for noninteracting systems. Generalizations involve twisted boundary conditions [20] or Green functions [21–25], and are challenging to use in experiments or exact simulations. Indirect signatures such as the closing of gaps [15] or the crossing of energy levels [26] require the experimental tuning of microscopic parameters.

TBIs show a unique response to topological defects such as dislocations [27, 28] or  $\pi$  fluxes [9, 10, 28]. The adiabatic insertion of a  $\pi$  flux gives rise to midgap *charge and spin fluxon states* which are exponentially localized near the flux [9, 10], see Fig. 1(a). The existence of these states is protected against interactions and disorder by TRS, and has been suggested as a bulk probe of the  $Z_2$  index [9, 10]. Fluxons can also be defined in situations where spin is not conserved [9, 10]. Electron-electron repulsion lifts the degeneracy of charge and spin fluxons, and the two degenerate spin fluxon states constitute a localized spin (referred to as a *spinon* to distinguish it from electronic spins) with  $S^z = \pm 1/2$  [9]. Dynamical  $\pi$  fluxes emerge in the context of fractionalized TBIs [9, 12].

In this Letter, we use exact quantum Monte Carlo

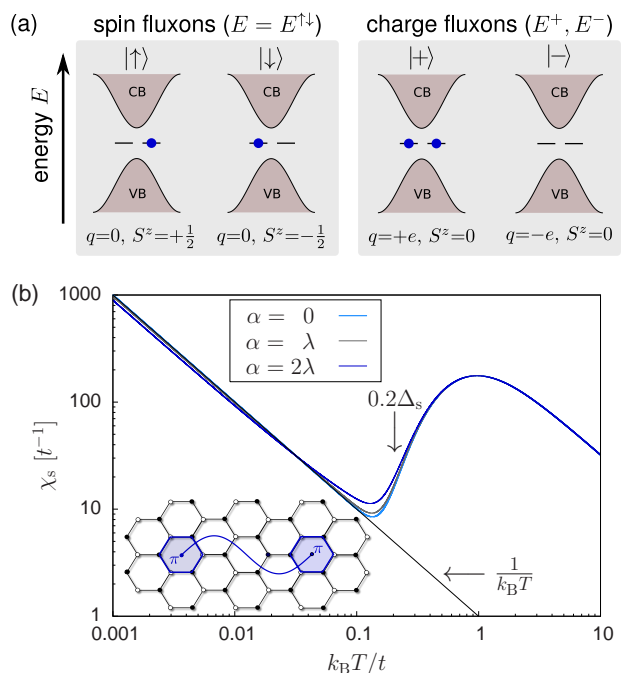


FIG. 1: (Color online) (a) Fluxons with charge  $q$  and spin  $S^z$  inside the TBI band gap [9, 10]. The spin fluxons form a Kramers doublet  $|\uparrow\rangle, |\downarrow\rangle$  with energy  $E^{\uparrow\downarrow}$ , and the charge fluxons  $|+\rangle, |-\rangle$  have energies  $E^+, E^-$ . (b) Inset: pair of  $\pi$  fluxes on the honeycomb lattice, connected by a branch cut. Main panel: spin susceptibility of the KM model ( $\lambda/t = 0.2$ ) with two  $\pi$  fluxes at maximal distance on an  $18 \times 18$  lattice, for different Rashba couplings  $\alpha$ . Also shown: spin gap energy scale  $0.2\Delta_s$  for  $T = 0$ ,  $\alpha = 0$ , and Curie law  $\frac{1}{k_B T}$ .

(QMC) simulations to demonstrate that  $\pi$  fluxes serve not only as a probe for correlated TBIs, but also permit the construction of quantum spin models of almost arbitrary geometry and with tunable, dynamical interactions. The spins correspond to spinons created by  $\pi$  fluxes, and the interaction is mediated by magnetic excitons.

We begin by considering the half-filled Kane-Mele (KM) model [3], with Hamiltonian [29]

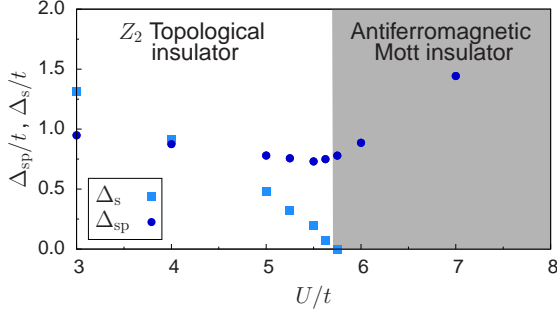


FIG. 2: (Color online) Spin gap  $\Delta_s$  (at wavevector  $\mathbf{q} = 0$ ) and single-particle gap  $\Delta_{\text{sp}}$  (at the Dirac point) in the thermodynamic limit as a function of the Hubbard repulsion  $U$ , at  $T = 0$  ( $\lambda/t = 0.2$ ,  $\alpha = 0$ ). The critical point is  $U_c/t = 5.70(3)$ . Errorbars are smaller than the symbols.

$$H_{\text{KM}} = -t \sum_{\langle i,j \rangle} \tau_{ij} \hat{c}_i^\dagger \hat{c}_j + i\lambda \sum_{\langle\langle i,j \rangle\rangle} \tau_{ij} \hat{c}_i^\dagger (\boldsymbol{\nu}_{ij} \cdot \boldsymbol{\sigma}) \hat{c}_j \quad (1)$$

$$+ i\alpha \sum_{\langle i,j \rangle} \tau_{ij} \hat{c}_i^\dagger (\mathbf{s} \times \hat{\mathbf{d}}_{ij}) \cdot \hat{\mathbf{z}} \hat{c}_j.$$

It describes nearest-neighbor electron hopping on the honeycomb lattice ( $t$ ), SO coupling ( $\lambda$ ) that reduces the  $SU(2)$  spin symmetry to a  $U(1)$  symmetry, and Rashba SO coupling ( $\alpha$ ) [30]. The factors  $\tau_{ij} = \pm 1$  account for  $\pi$  fluxes. We use  $t$  as the energy unit ( $\hbar = 1$ ), set  $\lambda/t = 0.2$ , and consider periodic systems with  $L \times L$  unit cells.

The model (1) can be solved exactly [3, 4]. For  $\alpha = 0$ , it describes a  $Z_2$  QSH insulator for any  $\lambda > 0$ . This state is characterized by a bulk band gap  $\Delta_{\text{sp}} = 3\sqrt{3}\lambda$ , a spin gap  $\Delta_s = 2\Delta_{\text{sp}}$ , and a quantized spin Hall conductivity  $\sigma_{xy}^s = \frac{e^2}{2\pi}$ . The topological state is stable for  $\alpha < 2\sqrt{3}\lambda$ .

On a lattice with periodic boundaries,  $\pi$  fluxes can only be inserted in pairs [see inset of Fig. 1(b)]. Each pair is connected by a branch cut, and every hopping process crossing the cut acquires a phase  $e^{i\pi} = -1$ , as encoded by  $\tau_{ij}$  in Eq. (1). Different choices of the branch cut for fixed flux positions are related by a gauge transformation.

In the topological phase of the model (1), each  $\pi$  flux gives rise to four fluxon states which are exponentially localized (due to the bulk energy gap  $\Delta_{\text{sp}}$ ) near the corresponding flux-threaded hexagons [9, 10], see Fig. 1. The spin fluxons  $|\uparrow\rangle, |\downarrow\rangle$  with energy  $E^{\uparrow\downarrow}$  form a Kramers pair related by TRS, and the charge fluxons  $|+\rangle, |-\rangle$  (with energies  $E^+, E^-$ ) are related by particle-hole symmetry. The fluxon states lie inside the bulk band gap, and for noninteracting electrons  $E^{\uparrow\downarrow} = E^+ = E^-$ .

The fluxons leave a characteristic signature in the temperature dependent spin and charge susceptibilities,

$$\chi_s = \beta \left( \langle \hat{M}_z^2 \rangle - \langle \hat{M}_z \rangle^2 \right), \quad \chi_c = \beta \left( \langle \hat{N}^2 \rangle - \langle \hat{N} \rangle^2 \right), \quad (2)$$

defined in terms of the operators of total spin in the  $z$  direction,  $\hat{M}_z = \sum_i \hat{c}_i^\dagger \sigma^z \hat{c}_i$ , and of total charge,  $\hat{N} =$

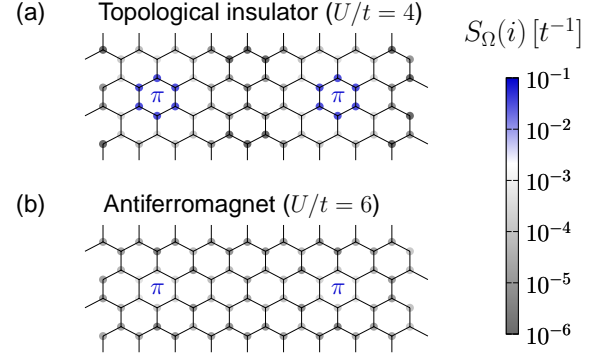


FIG. 3: (Color online) Integrated dynamical spin structure factor  $S_\Omega(i)$  (see text) at  $T = 0$  for the KMH model ( $L = 9$ ,  $\lambda/t = 0.2$ ,  $\alpha = 0$ ,  $\theta t = 40$ ) with two  $\pi$  fluxes. (a) TBI phase ( $U/t = 4$ ), (b) magnetic phase ( $U/t = 6$ ). Here  $\Omega = 0.2t$ .

$\sum_i \hat{c}_i^\dagger \hat{c}_i$ ; the inverse temperature is given by  $\beta = \frac{1}{k_B T}$ . At low temperatures  $k_B T \ll \Delta_{\text{sp}}$ , we can restrict the Hilbert space to  $\{|\uparrow\rangle, |\downarrow\rangle, |+\rangle, |-\rangle\}$ . If the spinons are independent, and for  $\alpha = 0$ , we expect a Curie law  $\chi_s = \chi_c = \frac{1}{2k_B T}$  per  $\pi$  flux, and hence  $\chi_s = \chi_c = \frac{1}{k_B T}$  for two independent  $\pi$  fluxes [29]. The prefactor of the Curie law follows from the quantized spin Hall conductance in the absence of Rashba coupling [3].

Figure 1(b) shows results for  $\chi_s$  as a function of temperature for the KM model with two  $\pi$  fluxes located at the largest possible distance. At temperatures  $k_B T \approx \Delta_s$ ,  $\chi_s$  is dominated by bulk effects. For  $k_B T \lesssim 0.1t$ , we recover the expected Curie law. The latter is robust with respect to Rashba coupling at least up to  $\alpha = 2\lambda$ , which is crucial for possible experimental realizations.

Figure 1(b) establishes the existence and thermodynamic signature of degenerate spin and charge fluxons in a QSH insulator threaded by a pair of  $\pi$  fluxes. To investigate the effect of electron-electron repulsion, we consider the *Kane-Mele-Hubbard (KMH) model* [31],

$$H_{\text{KMH}} = H_{\text{KM}} + H_U, \quad H_U = \frac{1}{2} U \sum_i (\hat{c}_i^\dagger \hat{c}_i - 1)^2. \quad (3)$$

Hamiltonian (3) with  $\alpha = 0$  has been studied intensely, see e.g. [15, 31–37], and is amenable to exact QMC methods [15, 32, 37]. The phase diagram includes a QSH insulating phase that is adiabatically connected to that of the  $U = 0$  KM model, and a Mott insulating phase with long-range, easy-plane antiferromagnetic order [37]. Figure 2 shows the quantum phase transition as a function of  $U/t$  at  $\lambda/t = 0.2$ . Magnetic correlations increase with  $U/t$ , and long-range order sets in at  $U_c/t = 5.70(3)$ . The transition has 3D XY universality [29, 37]. The closing of the extrapolated spin gap  $\Delta_s$  is tantamount to the condensation of magnetic excitons [36, 37]. For  $U \geq U_c$ , TRS is spontaneously broken, and the single-particle gap  $\Delta_{\text{sp}}$  remains open across the transition [37].

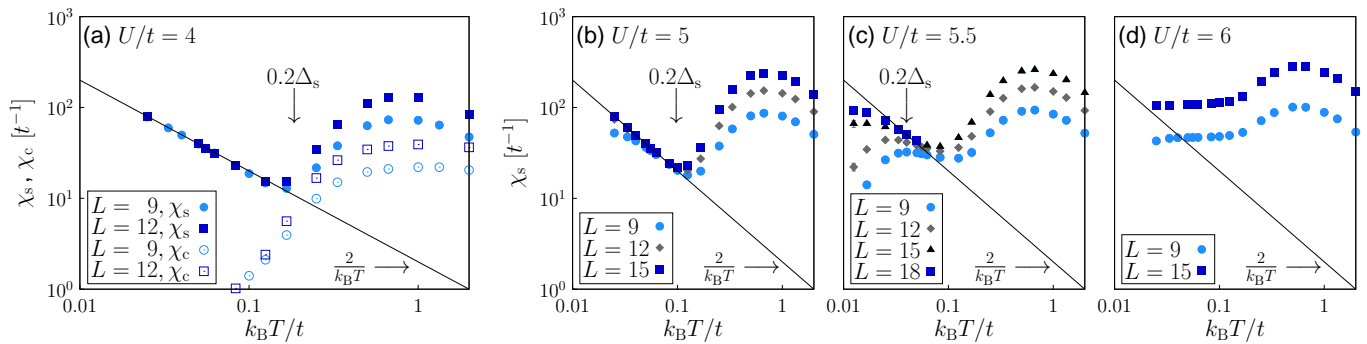


FIG. 4: (Color online) (a) Spin ( $\chi_s$ ) and charge ( $\chi_c$ ) susceptibilities of the KMH model ( $\lambda/t = 0.2$ ,  $\alpha = 0$ ) at  $U/t = 4$ . We consider  $L \times L$  lattices with two  $\pi$  fluxes placed at the maximal distance. (b)–(d)  $\chi_s$  as a function of temperature for different values of  $U/t$  ( $\lambda/t = 0.2$ ,  $\alpha = 0$ ). We also indicate the  $T = 0$  spin gap energy scale  $0.2\Delta_s$  and the Curie law  $\chi_s = \frac{2}{k_B T}$ .

The model (3) provides a test case for using  $\pi$  fluxes to probe a correlated TBI. We used a projective QMC method identical to Ref. [37] with projection parameter  $\theta t = 40$ , and a finite-temperature formulation [38]. In both cases, the Trotter discretization was chosen as  $\Delta\tau = 0.1$ . Including  $\pi$  fluxes does not cause a sign problem.

Spin fluxons can be detected by calculating the lattice-site resolved  $T = 0$  dynamical spin structure factor ( $H_{\text{KMH}}|n\rangle = E_n|n\rangle$ ,  $|0\rangle$ : ground state)

$$S(i, \omega) = \pi \sum_n |\langle n | \hat{c}_i^\dagger \sigma^z \hat{c}_i | 0 \rangle|^2 \delta(E_n - E_0 - \omega). \quad (4)$$

The integral of  $S(i, \omega)$  up to an energy scale  $\Omega/t = 0.2$  well within the charge gap  $\Delta_c \approx 2\Delta_{\text{sp}}$ ,  $S_\Omega(i) = \int_0^\Omega d\omega S(i, \omega)$ , yields a real-space map of the spin fluxon states  $|\uparrow\rangle, |\downarrow\rangle$ . For  $U/t = 4$ , corresponding to the QSH phase (see Fig. 2), and two  $\pi$  fluxes, we see in Fig. 3(a) very sharply defined spinons localized at the two flux-threaded hexagons. The value of  $S_\Omega(i)$  is about three orders of magnitude smaller at lattice sites which are further away from a flux, so that the spinons can easily be detected numerically. For the dependence of  $S_\Omega(i)$  on  $U/t$  see [29]. In Fig. 3(b), we show results for the magnetic insulating phase at  $U/t = 6$ . As expected for this topologically trivial state, and similar to the case without  $\pi$  fluxes, no spinons exist.

As for the noninteracting case [Fig. 1(c)], the spinons give rise to a characteristic Curie law in  $\chi_s$ . Figure 4(a) shows QMC results for the susceptibilities defined in Eq. (2) in the TBI phase ( $U/t = 4$ ). We again consider two  $\pi$  fluxes at the maximal separation. For  $k_B T \ll \Delta_s$ ,  $\chi_s$  is well described by  $\chi_s = \frac{2}{k_B T}$ , or  $\frac{1}{k_B T}$  per  $\pi$  flux. The factor of 2 compared to the case  $U = 0$  comes from the splitting of spin and charge states which only leaves the Kramers doublet  $\{|\uparrow\rangle, |\downarrow\rangle\}$  at low energies [29]. The Curie law holds down to the lowest temperatures in Fig. 4(a). Finally, due to the absence of low-energy charge fluxons as a result for the Hubbard repulsion,  $\chi_c$  is strongly suppressed at low temperatures.

Spinon-spinon interaction effects become visible for larger  $U/t$ , i.e., closer to the magnetic transition. Figures 4(b) and (c) show a deviation from the Curie law below a temperature scale determined by this interaction. In the model (3), the latter is mediated by the exchange of collective spin excitations (magnetic excitons), which are the lowest lying excitations of the correlated TBI phase (see Fig. 2), and evolve into the gapless Goldstone mode of the magnetic state. Since magnetic order is of the easy-plane type, the spinon-spinon interaction is expected to have the general form

$$S_{\text{int}} = -g^2 \sum_{\mathbf{r} \neq \mathbf{r}'} \iint_0^\beta d\tau d\tau' \times [\mathcal{S}_{\mathbf{r}}^+(\tau) D(\mathbf{r} - \mathbf{r}', \tau - \tau') \mathcal{S}_{\mathbf{r}'}^-(\tau') + \text{H.c.}], \quad (5)$$

where  $\mathcal{S}_{\mathbf{r}}^\pm(\tau)$  are spinon spin-flip operators acting at position  $\mathbf{r}$  at time  $\tau$ ,  $D(\mathbf{q}, i\Omega_m)$  is the exciton propagator ( $\mathbf{q}$ : momentum,  $\Omega_m = 2n\pi/\beta$ : bosonic Matsubara frequency), and  $g$  is a coupling constant. At long wavelengths, the dispersion relation of the collective spin mode can be written as  $\omega(\mathbf{q}) = \sqrt{v^2|\mathbf{q} - \mathbf{Q}|^2 + \Delta_s^2}$ , where  $v$  is the spin velocity,  $\Delta_s$  is the spin gap, and  $\mathbf{Q}$  is the magnetic ordering wavevector. The minimal exciton energy is  $\Delta_s$ . Fourier transformation [29] gives for low energies and long wavelengths

$$D(\mathbf{r}, \tau) \sim \exp(i\mathbf{Q} \cdot \mathbf{r}) \exp(-\Delta_s \tau) \exp\left(-\frac{|\mathbf{r}|^2 \Delta_s}{2v^2 \tau}\right). \quad (6)$$

The first term determines the sign of the interaction. The decay at large  $\tau$  is governed by  $\Delta_s$ . The fast decay as a function of  $|\mathbf{r}|$  underlies the clear Curie law seen, e.g., in Fig. 4. The interaction range and strength can be tuned via the spin gap and hence (cf. Fig. 2) via  $U/t$ .

From Eq. (6) we expect the *interaction range* to increase with  $U/t$  due to the decrease of  $\Delta_s$ , see Fig. 2. Indeed, Figs. 4(b),(c) reveal an enhanced effect of the spinon separation at low temperatures with increasing  $U/t$ . Close to the magnetic transition ( $U/t = 5.5$ ),

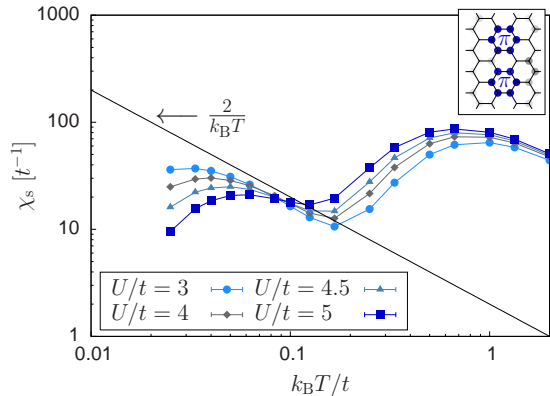


FIG. 5: (Color online) Spin susceptibility as a function of temperature for *two*  $\pi$  fluxes; see inset ( $\lambda/t = 0.2$ ,  $\alpha = 0$ ,  $L = 9$ ). Inset:  $S_\Omega(i)$  for  $U/t = 4$ , color coding as in Fig. 3.

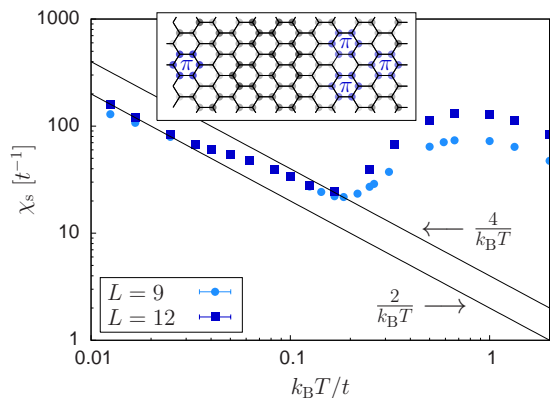


FIG. 6: (Color online) Spin susceptibility as a function of temperature for *four*  $\pi$  fluxes; see inset ( $\lambda/t = 0.2$ ,  $\alpha = 0$ ,  $U/t = 4$ ). Inset:  $S_\Omega(i)$  for  $L = 15$ , color coding as in Fig. 3.

Fig. 4(c) shows a two-spinon Curie law only for the largest system sizes ( $L = 18$ ). As  $U \rightarrow U_c$ , the interaction range diverges, and free spinons can no longer exist. For  $U > U_c$ , TRS is broken and  $\pi$  fluxes do not create spinons; the spin susceptibility in Fig. 4(d) is that of an antiferromagnet with a finite spin-wave density at  $T = 0$ .

To reveal the dependence of the spinon-spinon *interaction strength* on  $U$ , we consider two fluxes at a fixed, small distance (see inset of Fig. 5). We show  $\chi_s$  for different values of  $U/t$  in Fig. 5. For  $U/t = 3$ , a Curie law  $\chi_s \approx \frac{2}{k_B T}$  may be inferred at temperatures  $k_B T \approx 0.1t$ . Increasing  $U/t$ , the spinon-spinon interaction becomes too large to observe free spinons below the temperature range set by  $\Delta_s$ . The downturn of  $\chi_s$  occurs at higher and higher temperatures with increasing  $U/t$ , and reflects a tunable, correlation-induced energy scale of spinon-spinon interactions absent in Fig. 1(c).

The possibility of creating localized spinons with a tunable interaction mediated by magnetic excitons provides a toolbox to engineer interacting spin models in corre-

lated TBIs. The  $\pi$  fluxes can be arranged in almost arbitrary geometries, and the computational effort for our simulations does not depend on the number of fluxes.

As a proof of principle, we consider four spinons (i.e., two pairs of  $\pi$  fluxes), arranged so that three spinons form a ring, and the fourth spinon is located at the largest distance from the ring center. For large enough lattices, the separated spinon will not couple to the other three, and the physical problem is similar to experiments on coupled quantum dots [39] or flux qubits [40] in the context of quantum computation. The three spinons experience a transverse interaction of the form (5), and behave as an effective spin with  $S^z = \pm 1/2$  at low temperatures [29]. The spin susceptibility for  $U/t = 4$  shown in Fig. 6 reveals that, at low temperatures, the two independent spins indeed give rise to the expected Curie law  $\chi_s = \frac{2}{k_B T}$ . At higher temperatures  $k_B T \approx 0.1t$ , we find  $\chi_s = \frac{4}{k_B T}$ , corresponding to four independent spinons.

In the regime where  $\chi_s = \frac{2}{k_B T}$ , the sign of the spinon-spinon interaction determines the ground state degeneracy of the three-spin cluster. A net ferromagnetic interaction results in a spin-1/2 doublet, whereas an antiferromagnetic coupling gives rise to a four-fold degenerate, chiral ground state [29]. In principle, entropy measurements can be carried out to determine the sign of the exchange coupling for the case of Fig. 6. Since  $\mathbf{Q} = 0$  for the model (3), Eq. (6) suggests ferromagnetic coupling.

The possibility of constructing quantum spin models—which inherit the topological protection of their host—from  $\pi$  fluxes in correlated TBIs is generic. The interaction depends on the electronic Hamiltonian and the lattice geometry of the underlying TBI. Due to the SO interaction, the spin symmetry is  $U(1)$ , or  $Z_2$  with additional Rashba terms. We demonstrated that the  $\pi$ -flux spin models can be simulated numerically. However, our idea may also be realized experimentally. A strongly correlated TBI on the honeycomb lattice may be achieved with  $\text{Na}_2\text{IrO}_3$  [41] or with molecular graphene [42].  $\pi$  fluxes may be created via an adjacent superconductor and a magnetic field [10], or using SQUIDs. In solid state setups,  $\pi$  fluxes can also be created by dislocations [27, 28]. Exciting other recent proposals include artificial semiconductor honeycomb structures [43], cold atoms in optical lattices [18], and cold atoms on chips [44].

We thank N. Cooper, T. L. Hughes, L. Molenkamp, J. Oostinga, X.-L. Qi, C. Xu, and S. C. Zhang for insightful conversations. We acknowledge support from the DFG Grants No. FOR1162 and As 120/4-3, as well as generous computer time at the LRZ Munich and the JSC.

- 
- [1] J. E. Moore, *Nature* **464**, 194 (2010).
  - [2] M. Z. Hasan and C. L. Kane, *Rev. Mod. Phys.* **82**, 3045 (2010).

- [3] C. L. Kane and E. J. Mele, Phys. Rev. Lett. **95**, 146802 (2005).
- [4] C. L. Kane and E. J. Mele, Phys. Rev. Lett. **95**, 226801 (2005).
- [5] C. Wu, B. A. Bernevig, and S.-C. Zhang, Phys. Rev. Lett. **96**, 106401 (2006).
- [6] C. Xu and J. E. Moore, Phys. Rev. B **73**, 045322 (2006).
- [7] B. A. Bernevig, T. L. Hughes, and S. Zhang, Science **314**, 1757 (2006).
- [8] M. König, S. Wiedmann, C. Brüne, A. Roth, H. Buhmann, L. W. Molenkamp, X.-L. Qi, and S.-C. Zhang, Science **318**, 766 (2007).
- [9] Y. Ran, A. Vishwanath, and D.-H. Lee, Phys. Rev. Lett. **101**, 086801 (2008).
- [10] X.-L. Qi and S.-C. Zhang, Phys. Rev. Lett. **101**, 086802 (2008).
- [11] C.-Y. Hou, C. Chamon, and C. Mudry, Phys. Rev. Lett. **98**, 186809 (2007).
- [12] A. Rüegg and G. A. Fiete, Phys. Rev. Lett. **108**, 046401 (2012).
- [13] G. A. Fiete, V. Chua, X. Hu, M. Kargarian, R. Lundgren, A. Rüegg, J. Wen, and V. Zyuzin, Physica E **44**, 845 (2012).
- [14] Z. Y. Meng, T. C. Lang, S. Wessel, F. F. Assaad, and A. Muramatsu, Nature **464**, 847 (2010).
- [15] M. Hohenadler, T. C. Lang, and F. F. Assaad, Phys. Rev. Lett. **106**, 100403 (2011).
- [16] S. Raghu, X. Qi, C. Honerkamp, and S. Zhang, Phys. Rev. Lett. **100**, 156401 (2008).
- [17] D. Pesin and L. Balents, Nature Phys. **6**, 376 (2010).
- [18] B. Béri and N. R. Cooper, Phys. Rev. Lett. **107**, 145301 (2011).
- [19] K. Sun, W. V. Liu, A. Hemmerich, and S. D. Sarma, Nature Phys. **8**, 67 (2012).
- [20] Q. Niu, D. J. Thouless, and Y.-S. Wu, Phys. Rev. B **31**, 3372 (1985).
- [21] Z. Wang, X.-L. Qi, and S.-C. Zhang, Phys. Rev. Lett. **105**, 256803 (2010).
- [22] V. Gurarie, Phys. Rev. B **83**, 085426 (2011).
- [23] Z. Wang, X.-L. Qi, and S.-C. Zhang, arXiv:1201.6431v2 (2012).
- [24] Z. Wang and S.-C. Zhang, arXiv:1203.1028 (2012).
- [25] T. Yoshida, S. Fujimoto, and N. Kawakami, arXiv:1111.6250 (2011).
- [26] C. N. Varney, K. Sun, M. Rigol, and V. Galitski, Phys. Rev. B **84**, 241105 (2011).
- [27] Y. Ran, Y. Zang, and A. Vishwanath, Nature Phys. **5**, 298 (2009).
- [28] V. Juricic, A. Mesaros, R.-J. Slager, and J. Zaanen, Phys. Rev. Lett. **108**, 106403 (2012).
- [29] See Supplemental Material for more details.
- [30] Y. A. Bychkov and E. I. Rashba, J. Phys. C: Solid State Phys. **17**, 6039 (1984).
- [31] S. Rachel and K. Le Hur, Phys. Rev. B **82**, 075106 (2010).
- [32] D. Zheng, G.-M. Zhang, and C. Wu, Phys. Rev. B **84**, 205121 (2011).
- [33] C. Griset and C. Xu, Phys. Rev. B **85**, 045123 (2012).
- [34] S.-L. Yu, X. C. Xie, and J.-X. Li, Phys. Rev. Lett. **107**, 010401 (2011).
- [35] W. Wu, S. Rachel, W.-M. Liu, and K. Le Hur, arXiv:1106.0943 (2011).
- [36] D.-H. Lee, Phys. Rev. Lett. **107**, 166806 (2011).
- [37] M. Hohenadler, Z. Y. Meng, T. C. Lang, S. Wessel, A. Muramatsu, and F. F. Assaad, Phys. Rev. B **85**, 115132 (2012).
- [38] F. F. Assaad and H. G. Evertz, in *Computational Many Particle Physics*, Vol. 739 of *Lecture Notes in Physics*, edited by H. Fehske, R. Schneider, and A. Weiße (Springer Verlag, Berlin, 2008), p. 277.
- [39] L. Gaudreau, G. Granger, A. Kam, G. C. Aers, S. A. Studenikin, P. Zawadzki, M. Pioro-Ladriere, Z. R. Wasilewski, and A. S. Sachrajda, Nature Phys. **8**, 54 (2012).
- [40] A. Izmailkov, M. Grajcar, S. H. W. van der Ploeg, U. Hübner, E. Il'ichev, H.-G. Meyer, and A. M. Zagorskin, Europhys. Lett. **76**, 533 (2006).
- [41] A. Shitade, H. Katsura, J. Kunes, X.-L. Qi, S.-C. Zhang, and N. Nagaosa, Phys. Rev. Lett. **102**, 256403 (2009).
- [42] K. K. Gomes, W. Mar, W. Ko, F. Guinea, and H. C. Manoharan, Nature **483**, (2012).
- [43] A. Singha, M. Gibertini, B. Karmakar, S. Yuan, M. Polini, G. Vignale, M. I. Katsnelson, A. Pinczuk, L. N. Pfeiffer, K. W. West, and V. Pellegrini, Science **332**, 1176 (2011).
- [44] N. Goldman, I. Satija, P. Nikolic, A. Bermudez, M. A. Martin-Delgado, M. Lewenstein, and I. B. Spielman, Phys. Rev. Lett. **105**, 255302 (2010).

## Supplemental Material

### Kane-Mele model

The models considered here are defined on the honeycomb lattice realized by graphene. Following the conventions of Castro-Neto *et al.* [1], the basis vectors are given by

$$\mathbf{a}_1 = \frac{1}{2}a(3, \sqrt{3}), \quad \mathbf{a}_2 = \frac{1}{2}a(3, -\sqrt{3}), \quad (7)$$

and nearest-neighbor sites are connected by the vectors

$$\boldsymbol{\delta}_1 = \frac{1}{2}a(1, \sqrt{3}), \quad \boldsymbol{\delta}_2 = \frac{1}{2}a(1, -\sqrt{3}), \quad \boldsymbol{\delta}_3 = a(-1, 0), \quad (8)$$

see Fig. 7. The lattice is bipartite, and the two sublattices A and B give rise to two nonequivalent Dirac points

$$\mathbf{K} = \left( \frac{2\pi}{3a}, \frac{2\pi}{\sqrt{3}a} \right), \quad \mathbf{K}' = \left( \frac{2\pi}{3a}, -\frac{2\pi}{\sqrt{3}a} \right). \quad (9)$$

The original KM model (without  $\pi$  fluxes) is given by

$$H_{\text{KM}} = -t \sum_{\langle i,j \rangle} \hat{c}_i^\dagger \hat{c}_j + i\lambda \sum_{\langle\langle i,j \rangle\rangle} \hat{c}_i^\dagger (\boldsymbol{\nu}_{ij} \cdot \boldsymbol{\sigma}) \hat{c}_j + i\alpha \sum_{\langle i,j \rangle} \hat{c}_i^\dagger (\mathbf{s} \times \hat{\mathbf{d}}_{ij}) \cdot \hat{\mathbf{z}} \hat{c}_j. \quad (10)$$

Here we use the spinor notation  $\hat{c}_i^\dagger = (\hat{c}_{i\uparrow}^\dagger, \hat{c}_{i\downarrow}^\dagger)$ , where  $\hat{c}_{i\sigma}^\dagger$  is a creation operator for an electron in a Wannier state at site  $i$  with spin  $\sigma$ . The notation  $\langle i, j \rangle$  and  $\langle\langle i, j \rangle\rangle$  indicates that the sites  $i$  and  $j$  are nearest neighbors and next-nearest neighbors, respectively, and implicitly includes the Hermitian conjugate terms.

The SO term corresponds to a next-nearest neighbor hopping with a complex amplitude  $i\lambda$ , and has been derived from the SO coupling in graphene [3]. This hopping acquires a sign  $\pm 1$  depending on its direction, the sublattice, and the electron spin. This sign is encoded in  $(\boldsymbol{\nu}_{ij} \cdot \boldsymbol{\sigma})$ , where

$$\boldsymbol{\nu}_{ij} = \frac{\mathbf{d}_{ik} \times \mathbf{d}_{kj}}{|\mathbf{d}_{ik} \times \mathbf{d}_{kj}|}, \quad (11)$$

$\mathbf{d}_{ik}$  is the vector connecting sites  $i$  and  $k$ , and  $k$  is the intermediate lattice site involved in the hopping process from  $i$  to  $j$ . To achieve the coordinate independent representation used in Eq. (10), the vectors  $\mathbf{d}_{\alpha\beta}$  are defined in three dimensional space, although the  $z$  component vanishes. The vector  $\boldsymbol{\sigma}$  is defined by  $\boldsymbol{\sigma} = (\sigma^x, \sigma^y, \sigma^z)$ , where  $\sigma^x, \sigma^y, \sigma^z$  are the Pauli matrices. For example, we have  $\nu_{ij}^z = -1$  for  $i$  and  $j$  as indicated in Fig. 7(c), but  $\nu_{mn}^z = +1$ .

The last term in Eq. (10) is the Rashba SO interaction [3, 4]. It is defined in terms of the spin vector  $\mathbf{s} = \boldsymbol{\sigma}/2$ , and the unit vector  $\hat{\mathbf{d}}_{ij}$  which can be expressed in terms of the vectors  $\boldsymbol{\delta}_1, \boldsymbol{\delta}_2, \boldsymbol{\delta}_3$ . The conventions chosen here yield the critical value  $\alpha_c = 2\sqrt{3}\lambda$  for the closing of the SO gap, in agreement with the work by Kane and Mele [3, 4]. The Rashba coupling breaks the  $z \mapsto -z$  inversion symmetry, and has to be taken into account, for example, in the presence of a substrate. Because this term includes spin-flip terms, spin is no longer conserved. The Rashba term cannot be included in QMC simulations as it causes a sign problem.

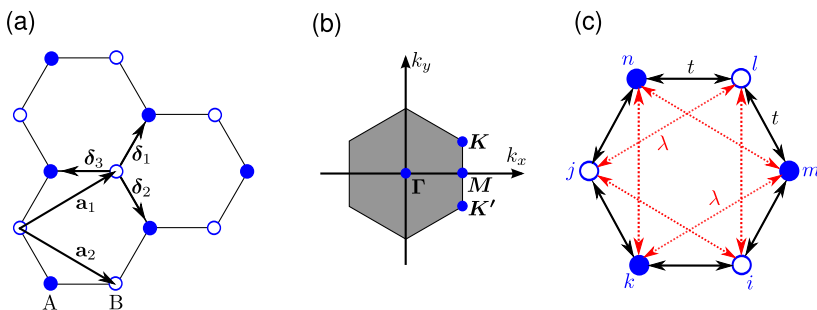


FIG. 7: (a) Basis vectors  $\mathbf{a}_1, \mathbf{a}_2$  and nearest-neighbor vectors  $\boldsymbol{\delta}_1, \boldsymbol{\delta}_2, \boldsymbol{\delta}_3$  of the honeycomb lattice. Filled and open circles symbolize lattice sites belonging to the two sublattices A and B. (b) Brillouin zone with the high-symmetry points  $\Gamma, M$  and the Dirac points  $\mathbf{K}, \mathbf{K}'$ . (c) A single hexagon of the honeycomb lattice, illustrating the nearest-neighbor hopping  $t$  and the SO interaction  $\lambda$  of the KM model.

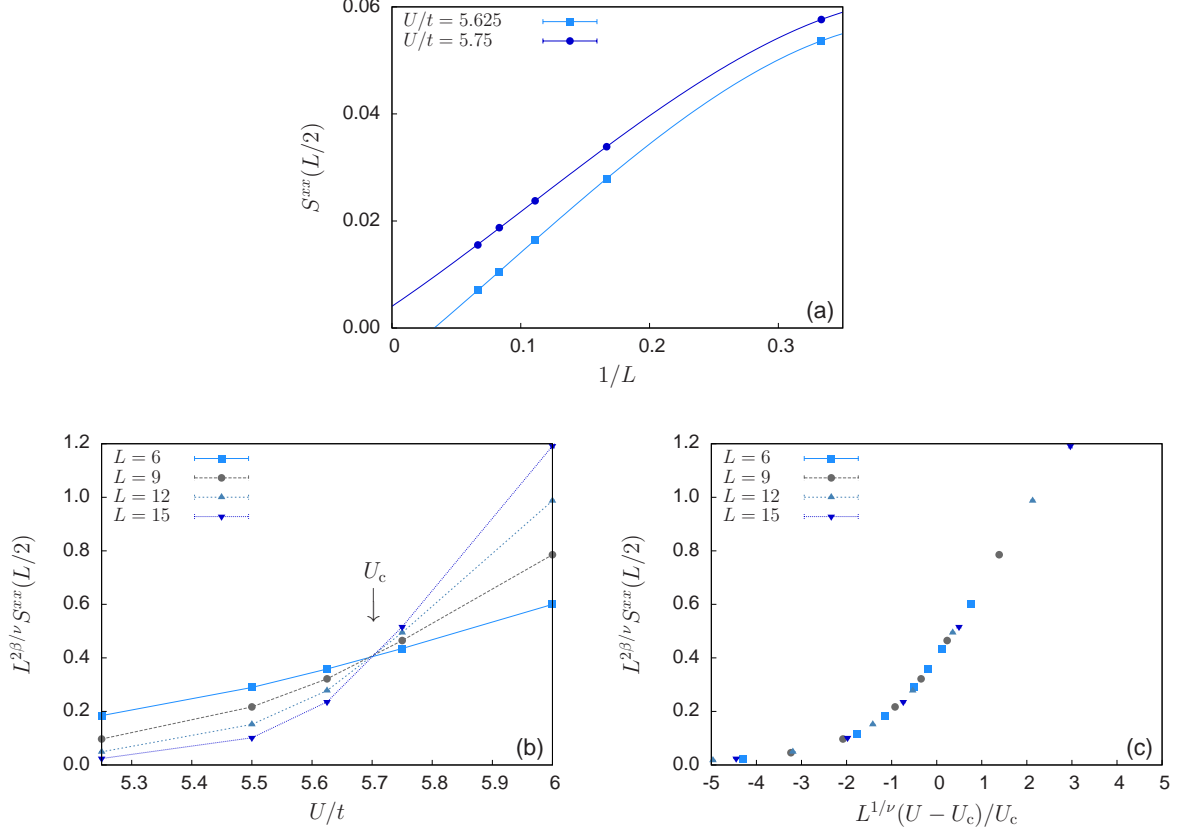


FIG. 8: (a) Finite-size extrapolation of the magnetic correlations in the  $x$  direction at the largest distance  $r = L/2$ , see Eq. (12), using third-order polynomial fits. The data reveal long-range order for  $U/t = 5.75$ , but not for  $U/t = 5.625$ . (b) Scaling of  $S^{xx}(L/2)$  using the critical exponents of the 3D XY model,  $z = 1$ ,  $\nu = 0.6717(1)$  and  $\beta = 0.3486(1)$  [2]. The intersect gives the critical value  $U_c/t = 5.70(3)$ , consistent with (a). (c) Scaling collapse obtained by using the 3D XY exponents and  $U_c/t = 5.70$ . Here  $\alpha = 0$ .

### Magnetic phase transition of the Kane-Mele-Hubbard model

The quantum phase transition between the TBI and the antiferromagnetic Mott insulator in the KMH model has first been found in mean-field theory [31]. The transition can also be studied using exact QMC simulations [15, 32, 37]. To minimize finite-size effects, we detect the onset of magnetic order from the real-space spin correlations

$$S^{xx}(r) = \langle S_A^x(r) S_A^x(0) \rangle \quad (12)$$

at the largest distance  $r = L/2$ . Here we consider correlations between spins on the A sublattice, but results are the same for the B sublattice. The limit  $\lim_{L \rightarrow \infty} S^{xx}(L/2)$  is identical to  $m^2$ , with  $m$  being the magnetization per site.

Figure 8(a) shows the extrapolation of  $S^{xx}(L/2)$ , revealing the absence of long-range order for  $U/t = 5.625$ , and the existence of long-range order at  $U/t = 5.75$ . These results provide an estimate of the critical point  $U_c$ . A more accurate value is obtained by considering the scaling behavior at the transition, which has previously been shown to fall into the 3D XY universality class [37]. Following Ref. 37, we plot  $L^{2\beta/\nu} S^{xx}(L/2)$  as a function of  $U$  for different system sizes using the critical exponents  $z = 1$ ,  $\nu = 0.6717(1)$  and  $\beta = 0.3486(1)$  [2]. Figure 8(b) reveals the expected intersect of curves at the critical point, and gives  $U_c/t = 5.70(3)$ . This value can be used to produce the scaling collapse of  $L^{2\beta/\nu} S^{xx}(L/2)$  as a function of  $L^{1/\nu}(U - U_c)/U_c$  shown in Fig. 8(c).

### Spinons as a probe of the topological state

Figure 9 shows the largest value of the spinon weight, as a function of  $U/t$ . A clear signal is found deep in the TBI phase, whereas a sharp drop is observed on approaching the magnetic phase transition at  $U_c/t = 5.70(3)$ . Hence, the spinon weight can be used in QMC simulations to track phase transitions which involve a change of the topological index.

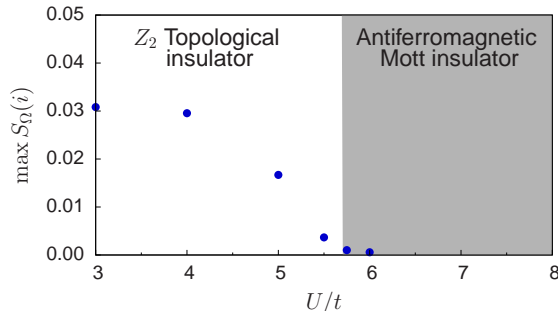


FIG. 9: Maximum of the integrated dynamical spin structure factor  $S_{\Omega}(i)$  as a function of  $U/t$ . Here  $\Omega/t = 0.2$ ,  $L = 9$ ,  $\alpha = 0$ , and  $\lambda/t = 0.2$ . The plot shows a clear spinon signal in the TBI phase, and a strong decrease in the vicinity of the magnetic transition at  $U_c/t = 5.70(3)$ .

### Spin susceptibility for two $\pi$ fluxes

A single  $\pi$  flux in a TBI gives rise to four states,  $|\uparrow\rangle, |\downarrow\rangle, |+\rangle, |-\rangle$ . In the absence of correlations, these states are degenerate. At low temperatures, the spin susceptibility can be calculated using the Hilbert space formed by only these states. Defining an effective Hamiltonian  $H_{\pi} = \sum_{\psi} E^{\psi} |\psi\rangle\langle\psi|$  with  $\psi \in \{+, -, \uparrow, \downarrow\}$  and  $E^{+} = E^{-} = E^{\uparrow} = E^{\downarrow} = E^{\uparrow\downarrow}$ , we obtain

$$\chi_s = \beta \left( \langle \hat{M}_z^2 \rangle - \langle \hat{M}_z \rangle^2 \right) = \frac{1}{k_B T} \frac{\sum_{\psi} \langle \psi | \hat{M}_z^2 e^{-\beta H_{\pi}} | \psi \rangle}{\sum_{\psi} \langle \psi | e^{-\beta H_{\pi}} | \psi \rangle} = \frac{1}{2k_B T}. \quad (13)$$

For  $U \gg k_B T$ , the spinons  $|\uparrow\rangle, |\downarrow\rangle$  are the only low-energy excitations, and  $\chi_s$  can be calculated by restricting  $\psi$  to  $\{\uparrow, \downarrow\}$ . Since  $E^{\uparrow} = E^{\downarrow} = E^{\uparrow\downarrow}$  due to TRS, we get

$$\chi_s = \frac{1}{k_B T}. \quad (14)$$

For the case of two independent  $\pi$  fluxes, the above results imply  $\chi_s = \frac{1}{k_B T}$  at  $U = 0$ , and  $\chi_s = \frac{2}{k_B T}$  for  $U > 0$ , in agreement with the QMC results.

Our derivation is only valid in the absence of Rashba SO coupling  $\alpha$ . However, the numerical results show that the low-temperature Curie law in  $\chi_s$  is the same also for  $\alpha \neq 0$ .

### Spin susceptibility and ground state degeneracy for four $\pi$ fluxes

The results for the KMH model with four  $\pi$  fluxes reveal a  $\frac{2}{k_B T}$  Curie law at low temperatures, and a  $\frac{4}{k_B T}$  Curie law at higher temperatures. This finding can be understood as corresponding to either two or four noninteracting spins. The latter correspond to the separate spinon and an effective spin-1/2 Kramers doublet (formed by the three nearby spins) in the regime where  $\chi_s \approx \frac{2}{k_B T}$ , and to four free spinons in the regime where  $\chi_s \approx \frac{4}{k_B T}$ .

The cluster formed by the three nearby spinons has the possible configurations

$$\begin{aligned} |M^z| = \frac{3}{2}: & \{ |\uparrow\uparrow\uparrow\rangle, |\downarrow\downarrow\downarrow\rangle \}, \\ |M^z| = \frac{1}{2}: & \{ |\uparrow\downarrow\downarrow\rangle, |\downarrow\uparrow\downarrow\rangle, |\downarrow\downarrow\uparrow\rangle, |\downarrow\uparrow\uparrow\rangle, |\uparrow\downarrow\uparrow\rangle, |\uparrow\uparrow\downarrow\rangle \}, \end{aligned} \quad (15)$$

where  $M^z$  denotes the total spin in the  $z$  direction. Since the exciton-mediated interaction in the KMH model promotes spin-flips, the ground state can be expected to have  $|M^z| = 1/2$ . The above mentioned effective spin-1/2 then corresponds to the two possible values  $M^z = \pm 1/2$ .

The degeneracy of the ground state depends on the sign of the interaction. Considering  $M^z = 1/2$ , we have the allowed states  $|\downarrow\uparrow\uparrow\rangle$ ,  $|\uparrow\downarrow\uparrow\rangle$  and  $|\uparrow\uparrow\downarrow\rangle$ . The spin-flip terms which connect these states are of the form  $J(S_i^+ S_{i+1}^- + S_i^- S_{i+1}^+)$ , with periodic boundary conditions. An equivalent representation is given by the Hamiltonian

$$H = J \sum_j (|j+1\rangle\langle j| + |j\rangle\langle j+1|), \quad (16)$$

which describes the hopping of a particle (the spin down) on a three-site ring, with  $|1\rangle = |\downarrow\uparrow\uparrow\rangle$  etc. The eigenstates are obtained by Fourier transformation, and have the form

$$|k\rangle = \frac{1}{\sqrt{3}} \sum_{j=1}^3 e^{ikj} |j\rangle, \quad k = 0, \pm \frac{2\pi}{3}. \quad (17)$$

The eigenvalues are given by

$$E(k) = 2J \cos k. \quad (18)$$

For  $J < 0$ , the ground state has  $k = 0$  and energy  $2J$ . For  $J > 0$ , the ground state is chiral, with  $k = \pm 2\pi/3$  and energy  $-J$ . Taking into account the sector  $M^z = -1/2$ , we find a total ground state degeneracy of *two* in the ferromagnetic case  $J < 0$ , and *four* in the antiferromagnetic case  $J > 0$ .

#### Fourier transform of the exciton propagator

The exciton propagator takes the form

$$D(\mathbf{q}, \tau) = \frac{e^{\tau\omega(\mathbf{q})}}{e^{\beta\omega(\mathbf{q})} - 1} - \frac{e^{-\tau\omega(\mathbf{q})}}{e^{-\beta\omega(\mathbf{q})} - 1} \quad (19)$$

with the exciton energy

$$\omega(\mathbf{q}) = \sqrt{v^2|\mathbf{q} - \mathbf{Q}|^2 + \Delta_s^2}. \quad (20)$$

In the low-temperature limit  $\beta \rightarrow \infty$ , the propagator becomes  $D(\mathbf{q}, \tau) = e^{-\tau\omega(\mathbf{q})}$ . Setting  $\mathbf{q}' = \mathbf{q} - \mathbf{Q}$ , the Fourier transform is given by

$$D(\mathbf{r}, \tau) = e^{i\mathbf{Q}\cdot\mathbf{r}} \int d^2q' e^{i\mathbf{q}'\cdot\mathbf{r}} e^{-\omega(\mathbf{q}'+\mathbf{Q})\tau}. \quad (21)$$

Assuming  $\Delta_s \gg v$ , we can expand to obtain  $\omega(\mathbf{q}' + \mathbf{Q}) \approx \Delta_s \left[ 1 + \frac{v^2|\mathbf{q}'|^2}{2\Delta_s^2} \right]$ . Taking the continuum limit, the Fourier transform involves the product of two Gaussian integrals, and the result is

$$D(\mathbf{r}, \tau) \sim \exp(i\mathbf{Q}\cdot\mathbf{r}) \exp(-\Delta_s\tau) \exp\left(-\frac{|\mathbf{r}|^2\Delta_s}{2v^2\tau}\right). \quad (22)$$

---

[1] A. H. Castro Neto, F. Guinea, N. M. R. Peres, K. S. Novoselov, and A. K. Geim, Rev. Mod. Phys. **81**, 109 (2009).

[2] M. Camprostrini, M. Hasenbusch, A. Pelissetto, P. Rossi, and E. Vicari, Phys. Rev. B **63**, 214503 (2001).